Faraday Discussions
Cite this: DOI: 10.1039/d5fd00149h

PAPER
View Article Online
View Journal

Effect of solvent structure on the Wien effect and ionic correlations at the nanoscale

Vincent Démery, [ab] Damien Toquer[c] and Hélène Berthoumieux *[a]

Received 4th December 2025, Accepted 22nd February 2026
DOI: 10.1039/d5fd00149h

In this study, we examine how the structure of the solvent affects the correlations and conductivity of moderately concentrated electrolytes. We describe polar solvents with a nonlocal permittivity, $\varepsilon(k)$, which we then incorporate into stochastic density functional theory (SDFT), focusing on ion transport in water. Using nonlocal SDFT and classical molecular dynamics simulations, we study the ionic hydration shell and its deformation under an electrostatic field. This allows us to identify the minimal ingredients required for an implicit solvent description to reproduce simulation results. As a perspective, we apply this framework to the transport of ions in a two-dimensional slab.

1 Introduction

The transport of ions in nanoconfined water is essential for biological processes as well as for technological applications. In such environments, electrolyte behaviour arises from the full molecular details of the system, making it crucial to extend our understanding of ion transport from macroscopic descriptions down to the nanoscale. Since the experiments conducted by Wien over a century ago,[1] we have known that the conductivity of bulk aqueous electrolytes increases for increasing electrostatic fields. The so-called first Wien effect was initially studied in a theoretical context by Debye, Hückel and Onsager (DHO),[2,3] who interpreted it as the destruction of the counterion cloud by the electrostatic field. Today, ionic conductivity is routinely measured in nanodevices. Recent experiments have revealed a more complex relationship between the applied field and conductivity than predicted by the DHO theory.[4–6] Fumagalli and co-authors[6] recently measured an abrupt increase in conductivity for highly confined systems and postulated that water's structural rearrangement is affected under molecular confinement.

[a]UMR CNRS Gulliver 7083, ESPCI Paris, PSL Research University, 75005 Paris, France. E-mail: helene.berthoumieux@espci.fr
[b]Univ Lyon, ENSL, CNRS, Laboratoire de Physique, F-69342 Lyon, France. E-mail: vincent.demery@espci.psl.eu
[c]Laboratoire de Physique de l'École Normale Supérieure, ENS, Université PSL, CNRS, Sorbonne Université, Université Paris Cité, Paris, France

While experiments can measure macroscopic properties such as conductivity, molecular dynamics (MD) simulations give access to microscopic observables, such as ion–ion and ion–water radial distribution functions.[7,8] Recently developed machine learning force fields can now incorporate the electronic properties of confinement walls into simulations.[9] These reveal an interplay between solvent structure, confinement, and the applied field, which governs ion transport. However, simulations do not provide a general equation that is valid at the nanoscale and governs the system.

In such a context, a great deal of theoretical work has been devoted to enhancing DHO by incorporating microscopic details.[10,11] Stochastic density functional theory (SDFT), a mathematical framework describing the overdamped dynamics of the density fluctuations of the different species,[12–14] has become a tool of choice for incorporating atomic structure. In the primitive version of SDFT, the solvent is implicit, characterised by its macroscopic permittivity, and the ions are described as point charges. This framework allows the derivation of Onsager's correction to the conductivity in a relatively straightforward manner.[3,13] First, the focus was on providing a better description of the ions, such as including the ionic size[15–17] or describing their hydrodynamic interactions.[18,19] Two strategies have been developed to improve solvent modelling. The first keeps the solvent implicit but enriches its response, for example, by including field-induced permittivity saturation in SDFT.[20] The second approach describes explicitly the water molecules as point dipoles, giving rise to coupled stochastic equations for water polarisation and ion density.[21] However, none of these approaches includes the dielectric correlations that arise from the hydrogen-bond network, which are crucial at the nanoscale.

The estimation of the effect of water structure on electrochemical features, such as ion solvation energy, is an old problem.[22,23] Nonlocal electrostatics, introduced in the 1970s to address this issue, models the solvent response through a wavenumber-dependent dielectric permittivity, $\varepsilon(k)$. In the late 1990s, nonlocal dielectric kernels fitted to classical MD simulations were proposed, capturing the spatially dispersive response of water and reproducing its short-range molecular ordering.[24–26] Recently, these kernels were used to model confined systems, accounting for the effects of water layering on the dielectric permittivity of nanoslabs,[27] the structure of electric double layers and hydration forces.[28]

In this study, we develop a theoretical framework to study the effect of water structure on ionic correlations. We incorporate wavenumber-dependent permittivity into SDFT. First, we analyse a simple model of a correlated medium and calculate the associated conductivity and pair correlation function. We then use a dielectric kernel developed for modelling water, compare our results with molecular dynamics (MD) simulations and identify the minimum requirements for capturing the effect of solvents on ion correlations. Finally, we extend our analysis to two-dimensional systems.

2 Nonlocal interactions and SDFT for conductivity and ionic correlations

We consider an aqueous electrolyte containing monovalent anions and cations with a charge $\pm e$ at a concentration n_0. When considering ionic interactions, the solvent can be described as a 'background', which screens the Coulomb

interaction through its macroscopic permittivity, ε. Here, we aim to include the effect of the molecular nature of water. One convenient way to do this is to introduce a nonlocal dielectric permittivity and to characterize the solvent by a kernel, $\varepsilon(k)$, depending on the wavenumber k in Fourier space, and such that the macroscopic limit $\varepsilon(k = 0) = \varepsilon$ is satisfied. In this case, the pair interaction between ion of species α and $\alpha' \in \{-1, 1\}$ in Fourier space is

$$V_{\alpha\alpha'}(k) = \alpha\alpha' e^2 G_0(k), \tag{1}$$

where $G_0(k)$ denotes the Green's function for the electrostatic interaction in the system and obeys

$$G_0(k) = \frac{1}{k^2\varepsilon(k)} = \frac{\tilde{g}(k)}{\varepsilon}, \tag{2}$$

with ε the macroscopic permittivity of the solvent. In real space, the interaction between an anionic and a cationic point-charge separated by a distance r is written as $U(r) = -e^2/(2\pi)^3\varepsilon_0\int d\boldsymbol{k} e^{-i\boldsymbol{k}\cdot\boldsymbol{r}} G_0(k)$. Now, the electrolyte is submitted to a constant external field $\boldsymbol{E}$. Starting from a description of the anions and cations as coupled overdamped Langevin particles, one can derive a stochastic density functional theory (SDFT). At temperature T, the ionic density fields n_α obey the equations:

$$\partial_t n_\alpha = -\nabla\cdot\boldsymbol{j}_\alpha, \tag{3}$$

$$\boldsymbol{j}_\alpha = -D_\alpha\nabla n_\alpha + \kappa_\alpha n_\alpha \boldsymbol{f}_\alpha + (2D_\alpha n_\alpha)^{1/2}\boldsymbol{\eta}_\alpha, \tag{4}$$

where κ_α is the mobility at infinite dilution, which is related to the diffusion coefficient D_α by the Einstein relation $D_\alpha = k_B T\kappa_\alpha$, with k_B the Boltzmann constant, and $\boldsymbol{\eta}_\alpha(\boldsymbol{x}, t)$ is a Gaussian white noise with correlation

$$\langle \boldsymbol{\eta}_\alpha(\boldsymbol{x},t)\boldsymbol{\eta}_{\alpha'}(\boldsymbol{x}',t')^T\rangle = \delta_{\alpha\alpha'}\delta(\boldsymbol{x} - \boldsymbol{x}')\delta(t - t'). \tag{5}$$

We have introduced the electrostatic force,

$$f_\alpha = \alpha e\boldsymbol{E} - \sum_{\alpha'}\nabla V_{\alpha\alpha'} * n_{\alpha'}, \tag{6}$$

with * the convolution over spatial variables. The average electrical current is given by $\langle \boldsymbol{J}\rangle = \sum_\alpha \alpha e\langle \boldsymbol{j}_\alpha\rangle$ and the conductivity is defined *via* $\langle \boldsymbol{J}\rangle = \sigma\boldsymbol{E}$. We introduce eqn (3) and (6) in the definition of $\langle \boldsymbol{J}\rangle$ and get

$$\langle \boldsymbol{J}\rangle = e^2\left(\sum_\alpha \kappa_\alpha n_0\right)\boldsymbol{E} - e\sum_{\alpha,\alpha'}\alpha\kappa_\alpha\left\langle n_\alpha\nabla V_{\alpha\alpha'} * n_{\alpha'}\right\rangle. \tag{7}$$

To rewrite the second term, we introduce density fluctuations and their stationary time correlations as

$$\delta n_\alpha(\boldsymbol{x},t) = n_\alpha(\boldsymbol{x},t) - n_0, \tag{8}$$

$$C_{\alpha\alpha'}(\boldsymbol{x}) = \langle \delta n_\alpha(\boldsymbol{x},t)\delta n_{\alpha'}(0,t)\rangle = n_0^2 h_{\alpha\alpha'}(\boldsymbol{x}). \tag{9}$$

The pair correlation $h_{\alpha\alpha'}(\boldsymbol{x})$ is proportional to the correlations $C_{\alpha\alpha'}(\boldsymbol{x})$ up to a delta function that we neglect here.[13] So, the ionic current $\langle \boldsymbol{J}\rangle$ is equal to

$$\langle \boldsymbol{J} \rangle = \sigma_0 \boldsymbol{E} - e n_0^2 \sum_{\alpha,\alpha'} \alpha \kappa_\alpha \int h_{\alpha\alpha'}(\boldsymbol{r}) \nabla V_{\alpha\alpha'}(\boldsymbol{r}) \mathrm{d}\boldsymbol{r}, \tag{10}$$

where $\sigma_0 = e^2 n_0 \sum_\alpha \kappa_\alpha$ is the conductivity in the absence of ionic interactions.

Assuming small density fluctuations, which correspond to the Debye–Hückel approximation, eqn (3) and (4) can be linearised and the out-of-equilibrium ionic density correlations can be computed. With the notations

$$\kappa = \kappa_+ + \kappa_-, \quad m^2 = \frac{2 n_0 e^2 \beta}{\varepsilon_0 \varepsilon}, \quad \boldsymbol{F} = \frac{\beta e \boldsymbol{E}}{m}, \tag{11}$$

where $\beta = 1/k_\mathrm{B}T$, m is the inverse of the Debye length and F a dimensionless field, the correlations can be written as

$$\tilde{h}_{++} = \frac{1}{n_0} \frac{\left(1 + \frac{m^2 \tilde{g}(k)}{2}\right)^2 + \left(\frac{m k_\parallel F}{k^2}\right)^2}{\left(1 + \frac{m^2 \tilde{g}(k)}{2}\right)\left[1 + m^2 \tilde{g}(k) + \left(\frac{m k_\parallel F}{k^2}\right)^2\right]} \tag{12}$$

$$\tilde{h}_{+-} = \frac{1}{n_0} \frac{m^2 \tilde{g}(k)}{2} \frac{\left(1 + \frac{m^2 \tilde{g}(k)}{2} - i\frac{m k_\parallel F}{k^2}\right)}{\left(1 + \frac{m^2 \tilde{g}(k)}{2}\right)\left[1 + m^2 \tilde{g}(k) + \left(\frac{m k_\parallel F}{k^2}\right)^2\right]}. \tag{13}$$

The component of $\boldsymbol{k}$ in the direction of the electrostatic field $\boldsymbol{E}$ is denoted by $k_\parallel$. The out-of-equilibrium ionic correlations $h_{\alpha,\alpha'}$ now depend on the molecular structure of the solvent, included in $\varepsilon(k)$ *via* the nonlocal Green's function $\tilde{g}$, defined in eqn (2). The local static limit of nonlocal SDFT ($\varepsilon(k) = \varepsilon$, $F = 0$) is the Debye–Hückel theory. Eqn (12) and (13) are valid in the limit of low field ($E \leq 0.1$ V nm^{-1}) ensuring an isotropic dielectric kernel.[20] Note that hard-core repulsion must be encoded at high concentrations, but approximate solutions are compatible with the SDFT framework.[15] Note that $\tilde{h}_{-+} = \tilde{h}_{+-}^*$ and $\tilde{h}_{--} = \tilde{h}_{++}$.

From eqn (10)–(13), we can calculate the electrostatic correction to conductivity, taking into account the solvent structure,

$$\frac{\Delta\sigma}{\sigma_0} = -\frac{\beta m^5 e^2}{2(2\pi)^2 \varepsilon \varepsilon_0} \int_0^\infty \mathrm{d}u \int_{-1}^1 \mathrm{d}y \frac{y^2 u^4 \tilde{g}^2 \left(1 + \frac{m^2}{2}\tilde{g}\right)}{u^2 (1 + m^2 \tilde{g})\left(1 + \frac{m}{2}\tilde{g}\right)^2 + \left(1 + \frac{m}{2}\tilde{g}\right)^2 F^2 y^2}, \tag{14}$$

where we have introduced the integration variables $u = k/m \in (0;\infty)$ and $y = k_\parallel/k \in (-1,1)$.

3 Simple model for a molecular solvent

In the 1950s, Schellman postulated that ionic interaction can increase at short distances in polar liquids such as water due to a reduction in ε.[29] This idea was later translated into a phenomenological model for the dielectric constant: the Lorentzian approximation:[22,30]

$$\varepsilon(k) = \varepsilon^* + \frac{\varepsilon - \varepsilon^*}{1 + \lambda^2 k^2}. \tag{15}$$

It is a simple model that interpolates between the molecular ranges associated with an "infrared" permittivity, $\varepsilon^* = \varepsilon(k \to \infty)$, and macroscopic distances associated with $\varepsilon = \varepsilon(k = 0)$. The characteristic length λ corresponds to the intermolecular orientation correlation length and is typically the size of a few solvent molecules.

Injecting $\varepsilon(k)$ in eqn (2), we compute the conductivity correction using eqn (14) for a nonlocal solvent as a function of the electrostatic field F for increasing polar correlation lengths λ. The results are presented in Fig. 1. The case of vanishing polar correlation lengths ($\lambda = 0$, purple plot) corresponds to a local solvent. As expected, $|\Delta\sigma/\sigma_0(F = 0)|$ increases with λ, which corresponds to an increase of the Wien effect. Indeed, over a shell of radius λ, the interaction increases as the solvent screens it with a low microscopic permittivity ε^*. As can be seen in Fig. 1, the effect is significant even for very small correlation lengths (green plot, $\lambda = 0.1$ nm), as the correction increases by a factor of 5. This illustrates the impact of ionic interactions over very short distances when describing the properties of electrolytes.

We now calculate the pair correlation $h_{-+}(x_{\parallel},x_{\perp})$ for different values of λ. The maps shown in Fig. 2 are obtained by inverting the Fourier transform correlation $\tilde{h}_{+-}$, given in eqn (12). Note that the integral of $\tilde{h}_{+-}$ is divergent at large $\boldsymbol{k}$ and we regularize it using a Gaussian cut-off function, $\exp(-l^2k^2/2)$.[13] The ionic pair correlation for a local solvent, characterized by its lone macroscopic permittivity ($\lambda = 0$), has already been studied. It was found that the probability of finding a counterion is higher in the direction of the field. This is indicated on the map by a red zone, which shows a higher concentration of counterions than the average one. In the direction perpendicular to the field (along $x_{\perp}$), a blue zone indicates a depletion of counterions compared to n_0.[13] Increasing the correlation length of the solvent λ induces a deformation of the correlation cloud, which becomes

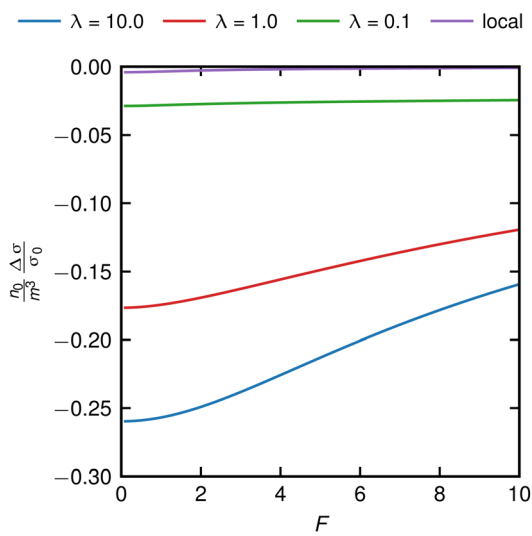

Fig. 1 Conductivity correction as a function of the dimensionless field, F, for $\varepsilon(k)$ given in eqn (15). We take $\varepsilon = 80$, $\varepsilon^* = 5$, $m = 1$ nm, and $n_0 = 0.1$ mol L^{-1}. The value of λ is expressed in nm.

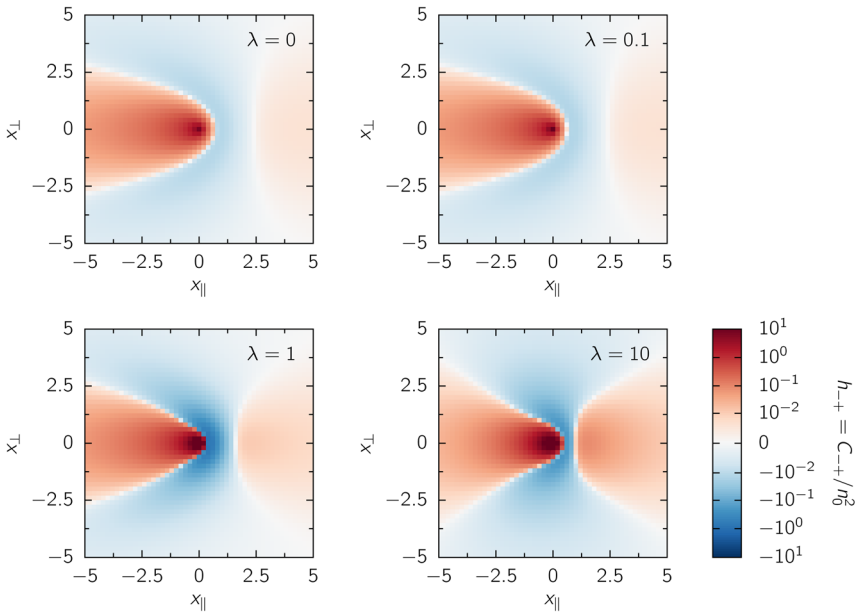

Fig. 2 Pair correlation function $h_{-+}(x_{\parallel},x_{\perp})$ from SDFT for different values of the correlation length λ. The maps are obtained for $F = 5$ and $m = 1\ \mathrm{nm}^{-1}$. The parameters for $\varepsilon(k)$ and n_0 are given in the caption of Fig. 1. The coordinates $x_{\parallel}$ and $x_{\perp}$, given in nm, denote the directions parallel and perpendicular, respectively, to the field direction.

visible when $\lambda > 1$, that is, when the correlation length of the solvent exceeds the Debye length. In this case, at distances shorter than λ, the effective permittivity is $\varepsilon^* < \varepsilon$, so that the effective inverse Debye length and dimensionless fields are $m^* > m$ and $F^* < F$. As a consequence, below the correlation length, the system behaves as if the distances were larger, $m^*r > mr$, since they are measured in units of the Debye length, and the field weaker, $F^* < F$. Beyond the correlation length and the Debye length, the correlations adopt a conical shape with an angle given by the dimensionless field F, independent of the small-scale permittivity.[31]

4 "Overscreening" solvents and the case of water

In the 1990s, the charge structure factor $S(k)$ for polar solvents was computed from MD simulation and experiments[32,33] and used to calculate $\varepsilon(k)$, the nonlocal permittivity of the solvents, using the fluctuation–dissipation theorem,[24,32,33]

$$\varepsilon(k) = \left(1 - \frac{\beta S(k)}{k^2\varepsilon_0}\right)^{-1}. \tag{16}$$

These results questioned the validity of the Lorentzian model, particularly in the context of water.[24,33] They showed that $\varepsilon(k)$ for water exhibits two poles on the k-axis, and is negative for $k \in [20\text{–}120]\ \mathrm{nm}^{-1}$. The negative range for $\varepsilon(k)$ is often referred to as "overscreening". Its molecular origin is a coupling between volume exclusion and orientation correlations, which are particularly important in water due to H-bonds.

The overscreening properties of nonlocal permittivity can be captured in a phenomenological model:

$$\varepsilon(k) = \varepsilon^* + \frac{\varepsilon - \varepsilon^*}{f(k)}, \quad f(k) = 1 - \frac{(k_1{}^2 + k_2{}^2)k^2 + k^4}{k_1{}^2 k_2{}^2}, \tag{17}$$

where k_1 and k_2 are the poles of $\varepsilon(k) - \varepsilon(k) < 0$ for $k \in [k_1,k_2]$ – that can be adjusted to fit MD data. ε is the macroscopic dielectric constant and ε^* is the permittivity at short range. This model is associated with two characteristic lengths for the solvent, which are defined as the poles of $1/\varepsilon(k)$, the kernel ruling the electrostatic interaction, given in eqn (2). One length encodes the oscillations of bound charges in water due to the layering of molecules around ions. The second length is the smearing length of the ion's electrostatic field, which is induced by correlated orientations of water dipoles.

First, we study the effect of the overscreening on the conductivity. The conductivity correction for different values of k_2 is plotted in Fig. 3. Compared to constant permittivity, we can see that overscreening leads to an increase in the Wien effect compared to the local model. However, the effect of nonlocality on bulk conductivity is weak, which is consistent with the good description of bulk experimental measurements with local models. Moreover, the overscreening effect is not monotonic with respect to the value of the second pole, k_2. Overscreening induces repulsion between ions of opposite charge, compensating for the increased ionic interaction at small distances due to low microscopic dielectric permittivity. Increasing the range of overscreening enhances this effect (from the blue curve to the red curve), until saturation is reached (from the red curve to the green curve).

We now study the effect of "overscreening" on the ionic pair correlation function $h_{-+}(x_\parallel,x_\perp)$, with the kernel $\varepsilon(k)$, eqn (17), parametrized to reproduce the

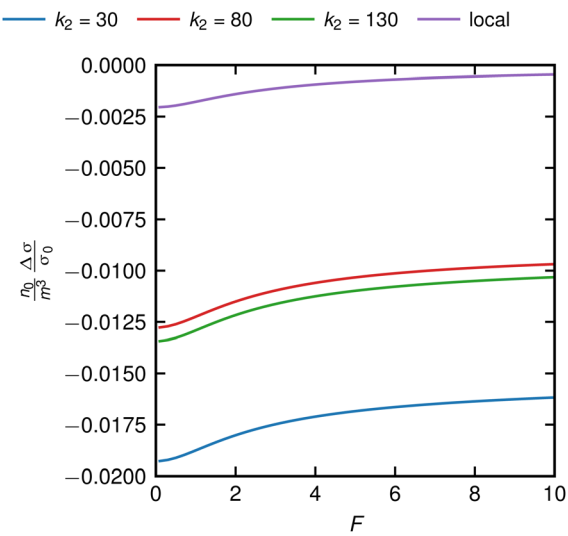

Fig. 3 Conductivity correction as a function of the dimensionless field, F, for $\varepsilon(k)$ given in eqn (17). We take $\varepsilon = 80$, $\varepsilon^* = 5$, $1/m = 1$ nm, and $n_0 = 0.1$ mol L^{-1}. k_1 is fixed to 25 nm^{-1}, and k_2 is expressed in nm^{-1}.

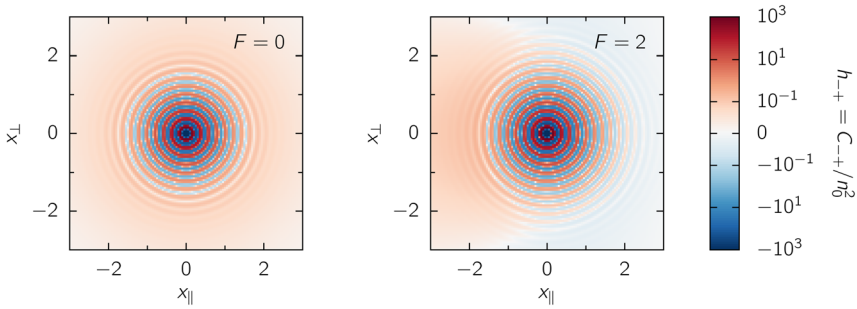

Fig. 4 Pair correlation function $h_{-+}(x_{\parallel},x_{\perp})$ from SDFT for $n_0 = 0.1$ mol L^{-1} and for $\varepsilon(k)$ given in eqn (17). The parameter values are $\varepsilon = 71$, $\varepsilon^* = 1$, $k_1 = 2.7$ nm^{-1}, and $k_2 = 41.7$ nm^{-1}.

nonlocal dielectric properties of the SPC/E water model.[27] The results are presented in Fig. 4.

The left panel corresponds to a vanishing electric field, $F = 0$. We see here a pattern of concentric circles of alternating sign around the origin. The amplitude of these oscillations diminishes significantly after 2 or 3 layers, but the pattern remains visible over a long distance. As a reminder, in the case of a featureless solvent characterized by its macroscopic permittivity, the correlation monotonously decays from the center to large distances. For a nonvanishing field, on the right panel, $F = 2$, we find the positive trail behind the ion, together with positive and negative oscillations centered on the ion, which indicate the layering of the solvent.

We performed classical MD simulations of a NaCl solution in water, at $n_0 = 0.150$ mol L^{-1}, under an electrostatic field $\boldsymbol{E} = E\boldsymbol{u}_x$.[20] Fig. 5 shows a snapshot of the simulations. We computed the correlation functions from these simulations. Details can be found in the Appendices. Fig. 6 (left panel) shows the pair correlation function $h_{-+}(\boldsymbol{r})$ for a dimensionless field, $F = 1.45$. As before, the red regions correspond to an accumulation of counterions, and blue regions

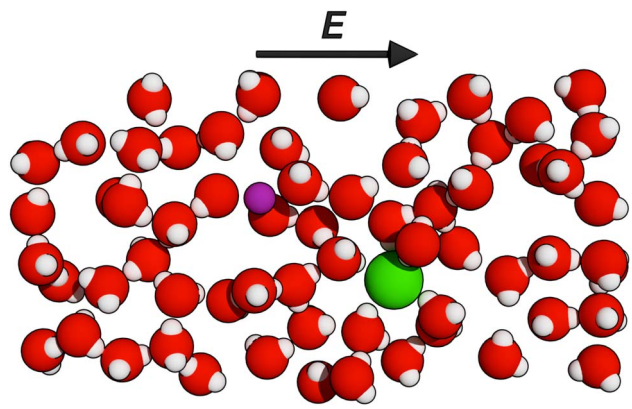

Fig. 5 Snapshot of the classical MD simulations. The sodium and chloride ions are represented by a purple and a green sphere, respectively. The external field is represented by the black arrow.

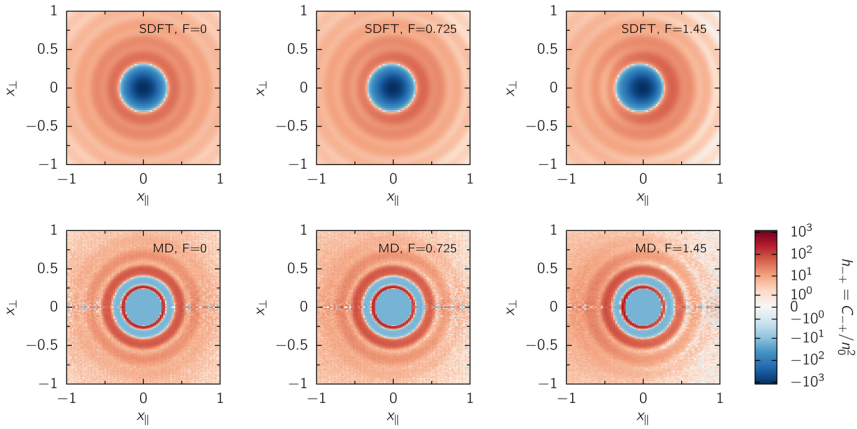

Fig. 6 Comparison of pair correlation functions obtained for SDFT calculations (top line) and MD simulations (bottom line) for $F = 0$ ($E = 0$ V nm^{-1}) for the first column, $F = 0.725$ ($E = 0.025$ V nm^{-1}) for the second column and $F = 1.45$ ($E = 0.05$ V nm^{-1}) for the third column. The form factor characterizing the ionic charge distribution is given in eqn (18). The parameter values for these maps are $n_0 = 0.150$ mol L^{-1} and $\eta = 10.5$ nm^{-1}, and the parameters for $\varepsilon(k)$ are given in the caption of Fig. 4.

correspond to a depletion of counterions, when compared to the mean concentration. We focus here on the solvation shell where the effect of the solvent is significant, *i.e.*, where $(x_\parallel, x_\perp) \leq 0.7$ nm. The central blue disk corresponds to the region of steric repulsion, which is modelled in MD simulations by the repulsive part of the Lennard-Jones interaction. The first fine red ring corresponds to an ion pair in direct contact. The second red ring, which corresponds to a distance of about 0.45 nm, is attributed to ions separated by one water molecule. In this case, oxygen is in contact with Na^+ and one hydrogen with Cl^-. After these two well-structured shells, the organisation becomes more blurred, but one can still see a depletion ring followed by an accumulation ring. The rings are not circular: the electrostatic field breaks the symmetry and slightly deforms them. The accumulation rings are broader and more pronounced for $x_\parallel > 0$, while the depletion rings are broader for $x_\parallel < 0$.

To compare the results of the MD simulations with the nonlocal SDFT, we incorporate $\varepsilon(k)$ from eqn (17) in eqn (13) and introduce a form factor $f(k)$ to model the spatial extension of the ions. Note that the parameters (ε, ε^*, k_1, k_2) for $\varepsilon(k)$ have been determined by fitting the MD data for bulk water.[27] For the sake of simplicity, we choose for $f(k)$ a Gaussian distribution:

$$f(k) = e^{-\frac{k^2}{2\eta^2}}. \tag{18}$$

The results are presented in Fig. 6. The top row represents the pair correlation maps computed with SDFT by Fourier inverting $f(k)^2 h_{-+}(k)$ for increasing values of the dimensionless field F. The second row corresponds to the pair correlation map measured from MD simulations for the same field amplitude. The left column represents the ionic correlations at equilibrium, in the absence of an applied external field. At the centre of the MD map, there is a blue exclusion zone due to Lennard-Jones repulsion between ions at short distances. This zone is surrounded by a narrow red ring corresponding to ion pairing. Then an

oscillation pattern appears: spherical depletion and accumulation over a distance of around 1 nm. Finally, a homogeneous accumulation can be seen at larger distances. The SDFT map (top map, left column) captures the central exclusion zone and the alternating rings. However, the absence of hard-core repulsion in the ionic interaction considered here leads to an incorrect description of the ion-pairing ring and the related depletion ring. The middle and right columns correspond to out-of-equilibrium correlations for increasing fields. For both MD simulations and SDFT predictions, we observe an asymmetry in the distribution, with depletion in the forward zone ($x_{\|} > 0$) and enrichment in the backward zone ($x_{\|} < 0$), which increases with F. SDFT provides an accurate prediction of the magnitude of this phenomenon. MD simulations show that the ion-pairing ring and the first solvation shell are almost unaffected by the external field, which is consistent with previous studies of the dielectric properties of the solvation shell.[34,35] At this stage of development, SDFT does not take into account dielectric saturation effects, and thus the solvent response is overestimated in the vicinity of the ion, as shown by the deformation of the first accumulation ring. Note that in this work, we focus on a minimal description of the system and choose a simple form factor. However, more detailed form factors could be considered, such as the smeared Born sphere, which have been shown to produce good results when combined with overscreening kernels for solvation energy.[23]

5 Nonlocal permittivity for 2D water

As shown in the previous section, SDFT theory using a nonlocal permittivity fitted to MD data, together with a form factor for the atomic charge distribution, is in reasonable agreement with MD simulations for both the structure of the shells and the amplitude of the correlations. We now apply this framework to 2D systems.

The nonlocal permittivity for 2D water has not been computed yet. To measure it, we have simulated a 2D layer of water (in the x,y-plane) between two graphene walls separated by a distance $h = 0.7$ nm, with classical MD force fields. The system is sketched in Fig. 7; details can be found in the Appendices. We introduce a 2D charge density for water as follows, $\rho(x,y) = 1/h\int dz \rho_{3D}(x,y,z)$, and define the charge structure factor in Fourier space as

$$S(k) = \frac{\langle \tilde{\rho}(k)\tilde{\rho}(-k)\rangle}{hL^2}, \quad k = \sqrt{{k_x}^2 + {k_y}^2}, \tag{19}$$

where $\tilde{\rho}(k)$ is obtained by Fourier transforming $\rho(x,y)$, and L is the lateral size of the slab. The function $S(k)/k^2$ for two-dimensional water is plotted in blue in Fig. 7, and the result for the bulk 3D system is plotted in red for comparison. As can be seen, the 2D correlations are close to the 3D ones for wavenumbers k corresponding to intermolecular distances, *i.e.*, $k \geq 10$ nm^{-1}. In particular, we observe a high maximum in $S(k)/k^2$ around $k \approx 30$ nm^{-1}, indicating layering of the charges and the phenomenon of "overscreening". At large distances, for $k \to 0$, we observe an increase in $S(k)/k^2$ for 2D water which is absent from the 3D signal. This behaviour indicates a screened Coulomb interaction between charges at long range.[35,36] This is due to a transition from an electric field confined by the graphene at short range to a 3D field at long range. Note that graphene modelled by MD simulations is a dielectric with $\varepsilon_G = 1$. It has been estimated that it confines the field over a dozen nanometers.[36]

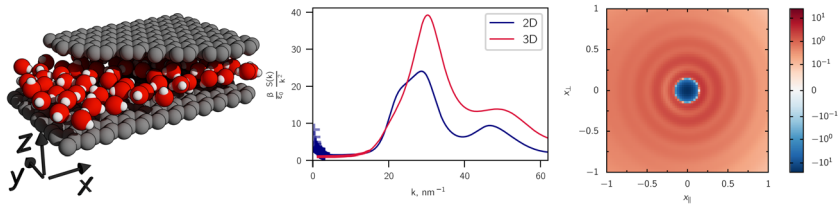

Fig. 7 (a) Snapshot of the classical MD simulations. Gray atoms: carbon, red atoms: oxygen, white atoms: hydrogen. (b) $\beta S(k)/\varepsilon_0 k^2 = 1 - 1/\varepsilon(k)$ (eqn (16)) as a function of the 2D wavenumber k for a 2D water density equal to 0.112 molecules per Å^2. (c) Ionic pair correlation function $h_{-+}(x_{\parallel}, x_{\perp})$ in a two-dimensional slab obtained for $F = 1$, $n_0 = 0.1$ mol L^{-1}, $\varepsilon(k)$ given in eqn (17) for parameter values given in the caption of Fig. 4, and a form factor, eqn (18), with $\eta = 15$ nm^{-1}.

At this stage, our point is not to be predictive of ionic correlation in 2D. Rather, it is to demonstrate that a well-parametrized nonlocal SDFT can be a powerful tool with which to study ion transport in confinement. To achieve this, we compute the 2D pair correlation function at short range using $\varepsilon(k)$ parametrized for bulk water, as we have just shown that charge correlations are similar for bulk water and a water slab at the molecular level. We invert the 2D Fourier transform of $f(k)^2 h_{-+}(k)$ and plot the corresponding pair correlation function in Fig. 7. Note that by doing so, we have neglected the long-range screening present in a 2D slab. The pattern is similar to that in 3D, but the depletion rings corresponding to ions separated by one water molecule are less pronounced. This is consistent with stronger electrostatic interactions and more significant ion pairing in 2D.[37]

6 Conclusions

In this work, we have shown that SDFT can be used to study ion transport in polar solvents. These solvents are correlated dielectric media characterized by a nonlocal permittivity $\varepsilon(k)$. Using the fluctuation–dissipation theorem, this kernel can be expressed as a function of the charge structure factor $S(q)$ of the solvent, easily computed from classical MD simulations. Over the years, analytical expressions for permittivity have been developed that enable the behaviour of aqueous solutions to be reproduced on a small scale. We have incorporated such a kernel into SDFT, and described the ion charge distribution by introducing a Gaussian form factor. Using this minimal framework, we have computed ionic pair correlations, which are in good agreement with those computed from MD simulations. Finally, we illustrate how nonlocal SDFT can be applied to 2D confined systems. A key point here is to use simulations at the relevant level of description to compute the dielectric kernel for confined water. The one we are using here, which employs classical MD simulations that ignore electronic effects and proton transfer, is probably not accurate enough to describe experiments.[6] However, for now, we will keep this approximation and compute the corresponding pair correlation function to demonstrate the possibilities of nonlocal SDFT for nanoconfined systems.

Conflicts of interest

There are no conflicts to declare.

Data availability

Data for this article, including data for correlation maps, are available at https://zenodo.org/records/18683322.

Appendices

Appendix: Simulations

Appendix: Simulation methods for bulk electrolytes. Simulations are performed using the GROMACS 2023 molecular dynamics simulation package.[38] Simulation boxes are periodically replicated in all directions, and long-range electrostatics are handled using the smooth particle mesh Ewald (SPME) technique with tin-foil boundary conditions. Lennard-Jones interactions are cut off at a distance $r_{\mathrm{cut}} = 0.9$ nm. The potential is shifted to zero at the cut-off separation. All systems are coupled to a heat bath at 300 K using the v-rescale thermostat with a time constant of 0.5 ps. We use MDAnalysis to treat the trajectories.

After creating the system, we first perform energy minimization. We then equilibrate the system in the *NVT* ensemble for 200 ps, and then in the NPT ensemble for another 200 ps using a Berendsen barostat at 1 bar. Production runs of 200 ns are performed in the *NVT* ensemble. The integration time step is set to $\Delta t = 2$ fs.

We simulate a cubic aqueous electrolyte box of size $L = 6.5$ nm. The 150 mmol solution contains 8875 water molecules and 25 ion pairs of (Na^+, Cl^-). We take the following LJ parameters ($\sigma_{\mathrm{Na}} = 0.231$ nm, $\varepsilon_{\mathrm{Na}} = 0.45$ kJ mol^{-1}) and ($\sigma_{\mathrm{Cl}} = 0.43$ nm, $\varepsilon_{\mathrm{Cl}} = 0.42$ kJ mol^{-1})[39] and we use the Lorentz–Berthelot mixing rules for the LJ interactions. We apply a static electrostatic field along the x-axis during the production run.

Appendix: Computation of the pair correlation function *h*. For each frame of the production run, we compute the separation distance $r_{i,j}$ for the 625 pairs of (Na^+, Cl^-). For each distance (x, r),$r = \sqrt{x^2 + y^2}$, we place +1 into the cylindrical bin such that $r \in [r_i, r_{i+1}]$, $x \in [x_i, x_{i+1}]$. We renormalise the bin density $H_{x,r}$ as follows:

$$h_{-+} = \frac{H_{x,r}}{V_{x,r} N_{\mathrm{Na}} n_{-} N_{\mathrm{frames}}} - 1, \tag{20}$$

with N_{frames} the number of treated frames, N_{Na} the number of ions of sodium in the simulation, n_- the concentration of chloride ions, and $V_{x,r}$ the volume of the bin.

Appendix: Simulation of the water slab. We have carried out classical force field molecular dynamics simulations of water molecules confined between 2 rigid walls. The walls are made of fixed carbon atoms on an hexagonal lattice, with a distance $d = 1.42$ Å between carbon atoms. Each sheet has an area of L^2, with $L = 199.26$ Å, the side size of the slab, and the sheets are spaced by a distance $h = 7$ Å, which defines the height of the slit. Vacuum is added on top of the system, leading to a total simulation box height of 500 Å. This avoids interactions with the periodic image along the direction of confinement. We have checked for consistency that changing this height only impacts the response at the lowest wavevector $k < 0.1$ Å^{-1}.

The simulations are performed using the GROMACS simulation package.[40] The 2D water density is set to 0.112 molecules per Å^2. The water is modelled using

the SPC/E water model[41] with the SETTLE algorithm,[42] and the water–carbon interaction parameters are taken from the GROMOS 53A6 parameter set.[43] These parameters have been shown to yield a reasonable description of water wetting on graphite and graphene.[44] We use a cutoff of 12 Å for both the Lennard-Jones and electrostatic interactions, and the long-range electrostatic contributions are simulated using the smooth particle mesh Ewald method.[45]

The trajectories are integrated with the velocity Verlet algorithm with a timestep of 1 fs, and the Bussi–Donadio–Parinello thermostat is used for temperature coupling.[46] The system is thermalized at 300 K for 1 ns, and is then simulated for 10 ns.

Appendix: Charge structure factor of 2D water. We introduce a 2D charge density for water as follows: $\rho(x,y) = h\int dz \rho_{3D}(x,y,z)$. We compute the charge structure factor in Fourier space as $S(k) = \langle\tilde{\rho}(k)\tilde{\rho}(-k)\rangle/hL^2$, with $k = \sqrt{{k_x}^2 + {k_y}^2}$ and where $\tilde{\rho}(k)$ is obtained by Fourier transforming $\rho(x,y)$. Note that for $k < 0.3$ Å^{-1}, we plot the susceptibility on the discrete wavevector $k_{mn} = \left(m\frac{2\pi}{L_x}, n\frac{2\pi}{L_y}\right)$. For $k >$ 0.3 Å^{-1} we smooth the susceptibility on close discrete wavevectors using a Gaussian kernel with a width $\sigma = 0.1$ Å^{-1}.

Notes and references

1 H. C. Eckstrom and C. Schmelzer, The Wien effect: Deviations of electrolytic solutions from Ohm's law under high field strengths, *Chem. Rev.*, 1939, **24**(3), 367–414.
2 P. Debye and E. Hückel, Theory of electrolytes—part ii: law of the limit of electrolytic conduction, *Phys. Z.*, 1923, **24**, 305–325.
3 L. Onsager, Report on a revision of the conductivity theory, *Trans. Faraday Soc.*, 1927, **23**, 341–349.
4 J. Cai, E. Griffin, V. H. Guarochico-Moreira, D. Barry, B. Xin, M. Yagmurcukardes, S. Zhang, A. K. Geim, F. M. Peeters and M. Lozada-Hidalgo, Wien effect in interfacial water dissociation through proton-permeable graphene electrodes, *Nat. Commun.*, 2022, **13**(1), 5776.
5 P. Robin, T. Emmerich, A. Ismail, A. Niguès, Y. You, G.-H. Nam, A. Keerthi, A. Siria, A. K. Geim, B. Radha and L. Bocquet, Long-term memory and synapse-like dynamics in two-dimensional nanofluidic channels, *Science*, 2023, **379**(6628), 161–167.
6 R. Wang, M. Souilamas, A. Esfandiar, R. Fabregas, S. Benaglia, H. Nevison-Andrews, Y. Qi, J. Normansell, P. Ares, G. Ferrari, A. Principi, A. K. Geim and L. Fumagalli, In-plane dielectric constant and conductivity of confined water, *Nature*, 2025, **646**, 606–610.
7 D. Lesnicki, C. Y. Gao, B. Rotenberg and D. T. Limmer, Field-dependent ionic conductivities from generalized fluctuation-dissipation relations, *Phys. Rev. Lett.*, 2020, **124**, 206001.
8 D. Lesnicki, C. Y. Gao, D. T. Limmer and B. Rotenberg, On the molecular correlations that result in field-dependent conductivities in electrolyte solutions, *J. Chem. Phys.*, 2021, **155**(1), 014507.
9 K. D. Fong, B. Sumić, N. O'Neill, C. Schran, C. P. Grey and A. Michaelides, The Interplay of Solvation and Polarization Effects on Ion Pairing in Nanoconfined Electrolytes, *Nano Lett.*, 2024, **24**(16), 5024–5030.

10 J.-F. Dufrêche, O. Bernard, S. Durand-Vidal and P. Turq, Analytical theories of transport in concentrated electrolyte solutions from the msa, *J. Phys. Chem. B*, 2005, **109**(20), 9873–9884.
11 J. J. Molina, *et al.*, Models of electrolyte solutions from molecular descriptions: The example of NaCl solutions, *Phys. Rev. E: Stat., Nonlinear, Soft Matter Phys.*, 2009, **80**, 065103.
12 D. S. Dean, Langevin equation for the density of a system of interacting Langevin processes, *J. Phys. A: Math. Gen.*, 1996, **29**(24), L613–L617.
13 V. Démery and D. S. Dean, The conductivity of strong electrolytes from stochastic density functional theory, *J. Stat. Mech. Theor. Exp.*, 2016, **2016**(2), 023106.
14 P. Illien, The Dean–Kawasaki equation and stochastic density functional theory, *Rep. Prog. Phys.*, 2025, **88**(8), 086601.
15 Y. Avni, R. M. Adar, D. Andelman and H. Orland, Conductivity of concentrated electrolytes, *Phys. Rev. Lett.*, 2022, **128**, 098002.
16 Y. Avni, D. Andelman and H. Orland, Conductance of concentrated electrolytes: Multivalency and the wien effect, *J. Chem. Phys.*, 2022, **157**(15), 154502.
17 O. Bernard, M. Jardat, B. Rotenberg and P. Illien, On analytical theories for conductivity and self-diffusion in concentrated electrolytes, *J. Chem. Phys.*, 2023, **159**(16), 164105.
18 A. Donev and E. Vanden-Eijnden, Dynamic density functional theory with hydrodynamic interactions and fluctuations, *J. Chem. Phys.*, 2014, **140**(23), 234115.
19 J.-P. Péraud, A. J. Nonaka, J. B. Bell, A. Donev and A. L. Garcia, Fluctuation-enhanced electric conductivity in electrolyte solutions, *Proc. Natl. Acad. Sci. U. S. A.*, 2017, **114**(41), 10829–10833.
20 H. Berthoumieux, D. Vincent and A. C. Maggs, Nonlinear conductivity of aqueous electrolytes: Beyond the first wien effect, *J. Chem. Phys.*, 2024, **161**(18), 184504.
21 P. Illien, A. Carof and B. Rotenberg, Stochastic density functional theory for ions in a polar solvent, *Phys. Rev. Lett.*, 2024, **133**, 268002.
22 A. A. Kornyshev, Nonlocal screening of ions in a structurized polar liquid — new aspects of solvent description in electrolyte theory, *Electrochim. Acta*, 1981, **26**, 1–20.
23 M. V. Fedorov and A. A. Kornyshev, Unravelling the solvent response to neutral and charged solutes, *Mol. Phys.*, 2007, **105**, 1–16.
24 P. A. Bopp, A. A. Kornyshev and G. Sutmann, Static Nonlocal Dielectric Function of Liquid Water, *Phys. Rev. Lett.*, 1996, **76**(8), 1280–1283.
25 A. C. Maggs and R. Everaers, Simulating nanoscale dielectric response, *Phys. Rev. Lett.*, 2006, **96**, 230603.
26 C. Shaff and S. Gekle, Dielectric response of the water hydration layer around spherical solutes, *Phys. Rev. E*, 2015, **92**, 032718.
27 G. Monet, F. Bresme, A. Alexeï Kornyshev and H. Berthoumieux, Nonlocal dielectric response of water in nanoconfinement, *Phys. Rev. Lett.*, 2021, **126**, 216001.
28 J. G. Hedley, H. Berthoumieux and A. A. Kornyshev, The dramatic effect of water structure on hydration forces and the electrical double layer, *J. Phys. Chem. C*, 2023, **127**, 8429–8447.

29 J. A. Schellman, The Application of the Bjerrum Ion Association Theory to the Binding of Anions By Protein, *J. Phys. Chem.*, 1953, **57**(4), 472–475.
30 A. A. Kornyshev, A. I. Rubinshtein and M. A. Vorotynstev, Model of non local electrostatics. i, *J. Phys. C Solid State Phys.*, 1976, **11**, 3307–3321.
31 H. Bonneau, D. Vincent and E. Raphaël, Stationary and transient correlations in driven electrolytes, *J. Stat. Mech.:Theory Exp.*, 2025, 033201.
32 O. F. Raineri, H. Resat and H. L. Friedman, Static longitudinal dielectric function of model molecular fluids, *J. Chem. Phys.*, 1992, **96**, 3068–3084.
33 A. K. Soper and M. A. Ricci, Structures of high-density and low-density water, *Phys. Rev. Lett.*, 2000, **84**, 2881.
34 H. Berthoumieux, G. Monet and R. Blossey, Dipolar Poisson models in a dual view, *J. Chem. Phys.*, 2021, **155**, 024112.
35 M. R. Becker, R. R. Netz, P. Loche, D. Jan Bonthuis, D. Mouhanna and H. Berthoumieux, Dielectric Properties of Aqueous Electrolytes at the Nanoscale, *Phys. Rev. Lett.*, 2025, **134**(15), 158001.
36 N. Kavokine, P. Robin and L. Bocquet, Interaction confinement and electronic screening in two-dimensional nanofluidic channels, *J. Chem. Phys.*, 2022, **157**(11), 114703.
37 D. Toquer, L. Bocquet and P. Robin, Ionic association and Wien effect in 2D confined electrolytes, *J. Chem. Phys.*, 2025, **162**(6), 064703.
38 B. Hess, C. Kutzner, D. van der Spoel and E. Lindahl, Gromacs 4: Algorithms for highly efficient, load-balanced, and scalable molecular simulation, *J. Chem. Theory Comput.*, 2008, **4**(3), 435–447.
39 P. Loche, P. Steinbrunner, S. Friedowitz, R. R. Netz and D. Jan Bonthuis, Transferable ion force fields in water from a simultaneous optimization of ion solvation and ion-ion interaction, *J. Phys. Chem. B*, 2021, **125**(30), 8581–8587.
40 M. Abraham, A. Alekseenko, B. Andrews, V. Basov, P. Bauer, H. Bird, E. Briand, A. Brown, M. Doijade, G. Fiorin, S. Fleischmann, S. Gorelov, G. Gouaillardet, A. Gray, M. Eric Irrgang, F. Jalalypour, P. Johansson, C. Kutzner, G. Łazarski, J. A. Lemkul, M. Lundborg, P. Merz, V. Miletić, D. Morozov, L. Müllender, J. Nabet, S. Páll, A. Pasquadibisceglie, M. Pellegrino, N. Piasentin, D. Rapetti, M. U. Sadiq, H. Santuz, R. Schulz, M. Shirts, T. Shugaeva, A. Shvetsov, P. Turner, A. Villa, S. Wingbermühle, B. Hess, and E. Lindahl. *GROMACS 2025.3 Manual*, Zenodo, 2025.
41 H. J. C. Berendsen, J. R. Grigera and T. P. Straatsma, The Missing Term in Effective Pair Potentials, *J. Phys. Chem.*, 1987, **91**(24), 6269–6271.
42 S. Miyamoto and P. A. Kollman, Settle: An analytical version of the SHAKE and RATTLE algorithm for rigid water models, *J. Comput. Chem.*, 1992, **13**(8), 952–962.
43 C. Oostenbrink, A. Villa, A. E. Mark and W. F. Van Gunsteren, A Biomolecular Force Field Based on the Free Enthalpy of Hydration and Solvation: The GROMOS Force-Field Parameter Sets 53A5 and 53A6, *J. Comput. Chem.*, 2004, **25**(13), 1656–1676.
44 S. R. Carlson, O. Schullian, M. R. Becker and R. R. Netz, Modeling Water Interactions with Graphene and Graphite via Force Fields Consistent with Experimental Contact Angles, *J. Phys. Chem. Lett.*, 2024, **15**(24), 6325–6333.

45 E. Ulrich, L. Perera, M. L. Berkowitz, T. Darden, H. Lee and L. G. Pedersen, A smooth particle mesh Ewald method, *J. Chem. Phys.*, 1995, **103**(19), 8577–8593.
46 G. Bussi, D. Donadio and M. Parrinello, Canonical sampling through velocity rescaling, *J. Chem. Phys.*, 2007, **126**(1), 014101.

